Journal of Environmental Chemical Engineering 14 (2026) 124647

Contents lists available at ScienceDirect

Journal of Environmental Chemical Engineering

journal homepage: www.elsevier.com/locate/jece

Concentration-dependent calcium polysulfide dosing for cadmium and zinc immobilization in contaminated groundwater

Jiwon Choi [a], Jin Chul Joo [b,*], Charles D. Shackelford [c], Kyoungphile Nam [d], Hyeon Woo Go [e], Dong Jun Kim [f], Won Seok Park [e]

[a] Department of Building and Urban Research, Korea Institute of Civil Engineering and Building Technology, Gyeonggi 10223, Republic of Korea
[b] Department of Civil and Environmental Engineering, Hanbat National University, Daejeon 34158, Republic of Korea
[c] Department of Civil and Environmental Engineering, Colorado State University, Fort Collins, CO 80523-1372, USA
[d] Department of Civil and Environmental Engineering, Seoul National University, Seoul 08826, Republic of Korea
[e] Beautiful Environmental Construction, CO., Ltd., Gyeonggi 13207, Republic of Korea
[f] Incheon & Gyeonggi Center, Korea Conformity Laboratories Materials Convergence Division, Incheon 21591, Republic of Korea

ARTICLE INFO

Keywords:
Cadmium
Calcium polysulfide (CPS)
Concentration-dependent dosing
Groundwater remediation
Metal immobilization
Metal sulfide precipitation
Zinc

ABSTRACT

A concentration-dependent dosing framework was developed for calcium polysulfide (CPS)-mediated immobilization of cadmium (Cd) and zinc (Zn) in acidic, smelting-impacted groundwater. Batch experiments were conducted using three groundwater samples representing low, intermediate, and high Cd and Zn concentrations. The effects of initial metal loading on CPS demand, sulfide supersaturation, metal removal, precipitate formation, and immobilization stability were evaluated using geochemical interpretation, mass balance, and extraction analysis. Dosing with CPS rapidly transitioned aqueous chemistry from oxidizing to reducing, sulfide-favorable conditions. However, substantial Cd and Zn precipitation occurred only after the metal-sulfide ion activity product exceeded the solubility threshold, defining a critical CPS dosage threshold ($C_{CPS,Cri}$). A slightly greater optimal CPS dosage ($C_{CPS,Opt}$) promoted sustained precipitation and reduced metal extractability. As the initial metal concentration increased, the optimal CPS-to-metal mass ratio decreased markedly from 15.9 to 1.46 for Cd and from 5.33 to 2.47 for Zn, indicating greater CPS utilization efficiency at higher metal loadings. Solid-phase characterization by SEM-EDS, TEM-EDS, XRD, and XPS identified crystalline $ZnS_{(s)}$, elemental sulfur, and Ca-bearing gypsum. Although crystalline $CdS_{(s)}$ was not resolved by XRD, Cd immobilization was evidenced by up to 99.7% aqueous Cd removal. Overall, the extractable metal fraction decreased with increasing initial metal concentration, indicating that immobilization stability depended on both CPS stoichiometry and supersaturation-controlled nucleation and precipitate growth. These findings demonstrate that CPS dosage should be based on both metal loading and site-specific geochemical demand rather than only stoichiometric sulfide requirements.

1. Introduction

Groundwater at mine smelting facilities frequently is impacted by persistent heavy-metal contamination derived from ore extraction and metallurgical processing, resulting in long-term geochemical impacts on adjacent soils and aquatic systems [1,2]. Among these metal contaminants, cadmium (Cd) and zinc (Zn) are of particular concern because Cd and Zn are abundant by-products of non-ferrous metal smelting and exhibit high mobility and persistence under diverse hydrogeochemical conditions [3,4]. Both speciation and phase partitioning of Cd and Zn are controlled by pH, redox potential, competing ions, mineral interfaces, and organic ligands, which collectively regulate long-term persistence across aqueous and solid phases [5,6]. As a consequence, Cd- and Zn-contaminated groundwater poses serious environmental risks including threats to aquatic systems, food safety and human health when used for agricultural or domestic purposes [5,7].

Because dissolved metal contaminants cannot be degraded, remediation generally depends on speciation transition, phase transfer, or immobilization rather than destructive transformation. Conventional *ex situ* approaches such as pump-and-treat, membrane separation, and ion exchange can reduce dissolved metal concentrations, but field performance often is constrained by aquifer heterogeneity, long remediation

* Corresponding author.
E-mail address: jincjoo@hanbat.ac.kr (J.C. Joo).

https://doi.org/10.1016/j.jece.2026.124647
Received 28 May 2026; Received in revised form 31 July 2026; Accepted 14 August 2026
Available online 16 August 2026

timeframes, membrane fouling, and secondary waste generation [8–10]. Consequently, *in situ* immobilization approaches whereby redox manipulation and mineral precipitation isolate metals from the biosphere through stable-phase transformation rather than groundwater extraction have emerged as viable alternatives [11,12].

Among *in situ* chemical remediation reagents, sulfur-bearing compounds and iron-based reductants have been evaluated extensively for immobilizing metal contaminants through redox transformation, sulfide complexation, and precipitation of sparingly soluble metal sulfides [13–15]. Representative reagents include iron sulfides (FeS/FeS_x), ferrous iron-based reductants, sodium dithionite ($Na_2S_2O_4$), and calcium polysulfide (CaS_x or CPS) [12–17]. Among these reagents, CPS has been shown to be particularly attractive for field-scale injection, because CPS is highly soluble, strongly reducing, and capable of supplying reactive sulfur species under subsurface conditions [12,16–23].

Upon injection, CPS undergoes hydrolysis and sulfur-speciation reactions to produce polysulfide, hydrosulfide, sulfide, and intermediate sulfur species, including HS^-/H_2S, S_x^{2-}, and $S_2O_3^{2-}$ [13,18]. These sulfur species react with dissolved divalent metal ions (Me^{2+}) to form metal sulfide precipitates ($MeS_{(s)}$), provided the ionic activity product (IAP_{MeS}) exceeds the solubility product constant ($K_{sp,MeS}$), where IAP_{MeS} and $K_{sp,MeS}$ are defined as follows:

$$IAP_{MeS} = \{Me^{2+}\}\{S^{2-}\} \quad (1)$$

and

$$K_{sp,MeS} = \{Me^{2+}\}_{eq}\{S^{2-}\}_{eq} \quad (2)$$

where $\{Me^{2+}\}_{eq}$ and $\{S^{2-}\}_{eq}$ are the thermodynamic activities of free divalent metal ions and sulfide ions, respectively, in equilibrium with the corresponding metal sulfide solid phase, and $K_{sp,MeS}$ is the solubility product constant for a given $MeS_{(s)}$. Because metal sulfides, particularly $CdS_{(s)}$ and $ZnS_{(s)}$, typically exhibit substantially lower solubility than the corresponding hydroxide or carbonate phases, CPS-induced sulfidation can promote more persistent immobilization and lower susceptibility to re-dissolution under appropriately controlled geochemical conditions [13–15,24].

Despite these advantages, most CPS-based remediation studies have focused primarily on the reductive immobilization of hexavalent chromium (Cr^{6+}) [12,16,17,25]. In contrast, mechanistic and design-oriented applications to redox-inert divalent metals such as Cd^{2+} and Zn^{2+} remain limited, particularly for field-derived groundwater with mixed-metal chemistries. For example, recent studies have demonstrated the feasibility of CPS-induced metal immobilization in homogeneous porous media, concentration-screening batch systems, and site-specific column configurations [19–23]. However, these studies have been limited to empirical dosage information, such that more generalized practical guidance for predicting CPS requirements across different metal concentration regimes at the field scale remains insufficient.

Building on these aforementioned studies, the present work advances CPS-based remediation from empirical dosage selection toward a mechanistically grounded, concentration-dependent dosing framework. Specifically, this study links dissolved metal concentration, sulfide availability, supersaturation, nucleation behavior, and post-remediation stability by defining a critical CPS precipitation-onset threshold, $C_{CPS,Cri}$, and an operational optimal dosage, $C_{CPS,Opt}$, based on coupled geochemical response, residual metal removal, and diminishing benefit of additional CPS addition. The central hypothesis is that CPS-induced immobilization is governed by both the stoichiometric sulfide demand and whether the IAP_{MeS} of a dissolved metal and reduced sulfur species exceeds the supersaturation threshold required for nucleation and subsequent growth of stable $MeS_{(s)}$. This framework is evaluated experimentally on the basis of laboratory batch experiments by relating CPS dosage to Cd and Zn removal behavior, mineralogical and surface-chemical characteristics of the resulting precipitates, and resistance of these precipitates to post-remediation extraction.

The proposed framework was evaluated using site-specific groundwaters representing low, intermediate, and high metal concentrations that were collected from multiple monitoring wells located within a single smelting-impacted site. Experimental evaluation linked CPS dosage to geochemical responses, residual aqueous metal concentrations, solid-phase mineralogical and surface-chemical compositions, mass balance behavior, and post-remediation extractability. The specific objectives of this study were to: (1) identify the critical precipitation-onset CPS threshold ($C_{CPS,Cri}$) and the operational optimum CPS dosage ($C_{CPS,Opt}$) required for Cd and Zn removal under varying concentration regimes; (2) determine whether CPS-derived precipitates contain sulfide-associated Cd and Zn phases using complementary solid-phase characterization techniques; (3) evaluate the stability and retention behavior of immobilized metals using acid extraction and sequential extraction analyses; and (4) develop a concentration-adjusted CPS dosing framework for mixed-metal groundwater systems.

The significance of this study lies in advancing CPS treatment from empirical dose selection toward a concentration-dependent dosing framework. By distinguishing the operational critical dosage, $C_{CPS,Cri}$, from the optimum dosage, $C_{CPS,Opt}$, and linking these thresholds to metal concentration, precipitate characteristics, and extractability, the results of this study provide a practical basis for site-specific CPS optimization. The results further show that CPS demand cannot be predicted solely from stoichiometry, but also must consider groundwater chemistry and supersaturation behavior. Accordingly, the proposed framework supports concentration-adjusted CPS screening and dose optimization in field-derived mixed-metal groundwaters.

2. Background

Upon dilution and injection into groundwater, CPS undergoes hydrolysis, dissociation, and redox-dependent sulfur-speciation reactions, generating several reactive sulfur species, including hydrosulfide (HS^-), hydrogen sulfide (H_2S), sulfide (S^{2-}), thiosulfate ($S_2O_3^{2-}$), and elemental sulfur (S^0), that depend on pH, dissolved oxygen (DO) concentration, oxidant demand, and groundwater composition [13,15,18,25]. The distribution of reduced sulfide species is governed primarily by pH-dependent acid-base equilibria (see Fig. S1), where H_2S is favored under acidic to near-neutral conditions ($pH < 7$), HS^- dominates from circumneutral to strongly alkaline conditions ($7 \leq pH \leq 13$), and S^{2-} becomes increasingly important only at very high $pH > 13$ near or above the second dissociation constant of H_2S. Because HS^- is the dominant dissolved sulfide species over circumneutral to strongly alkaline pH ranges [13], $MeS_{(s)}$ precipitation should not be interpreted as being controlled solely by free S^{2-} concentration. Instead, the precipitation potential reflects the combined effects of total sulfide availability, pH-dependent sulfide speciation, metal complexation, and the saturation state with respect to $MeS_{(s)}$ formation [13–15].

These reduced sulfur species can react with dissolved Cd^{2+} and Zn^{2+} to form sparingly soluble $MeS_{(s)}$ when IAP_{MeS} exceeds $K_{sp,MeS}$ of the corresponding sulfide phase. The saturation state is expressed as $\Omega_{MeS} = IAP_{MeS}/K_{sp,MeS}$ [13], where the magnitude of Ω_{MeS} determines the driving force for nucleation and crystalline growth, and $\Omega_{MeS} > 1$ defines thermodynamic supersaturation. Near-critical supersaturation ($\Omega_{MeS} \leq 1$) may result in incomplete or kinetically limited precipitation, whereas higher Ω_{MeS} lowers the nucleation energy barrier and promotes rapid formation and growth of $CdS_{(s)}$ and $ZnS_{(s)}$. Thus, CPS dosage can be linked directly to reduced sulfur availability, Ω_{MeS} development, nucleation behavior, and the immobilization potential of dissolved metals.

Metal sulfides generally exhibit substantially lower solubility than the corresponding metal hydroxides, providing a thermodynamic basis for sulfide-mediated immobilization of divalent metals such as Cd^{2+} and Zn^{2+} [13–15]. However, the stability of $MeS_{(s)}$ depends on pH, redox

potential, sulfide activity, competing ligands, crystallinity, and oxidative aging [13–15,24]. As a result, Cd- and Zn-bearing sulfide phases can remain sparingly soluble under reducing, sulfide-bearing conditions, but may undergo partial remobilization when dissolved oxygen or oxidation-reduction potential (ORP) increases or when pH decreases [5, 13–15]. Therefore, CPS treatment should be regarded as condition-dependent immobilization rather than irreversible stabilization.

Several reaction pathways govern CPS transformation, sulfide speciation, and $MeS_{(s)}$ precipitation. First, for CPS transformation and sulfur release, the following reactions are relevant:

$$CaS_x + \frac{3}{2}O_2 \rightarrow CaS_2O_3 + (x-2)S^0 \quad (3)$$

$$CaS_x + CO_2 + H_2O \rightarrow CaCO_{3(s)} + H_2S_{(aq)} + (x-1)S^0 \quad (4)$$

Second, sulfide-mediated precipitation of divalent metals is represented as follows:

$$Me^{2+} + H_2S \leftrightarrow MeS_{(s)} + 2H^+ \quad (5)$$

$$Me^{2+} + HS^- \leftrightarrow MeS_{(s)} + H^+ \quad (6)$$

$$Me^{2+} + S^{2-} \leftrightarrow MeS_{(s)} \quad (7)$$

Next, pH-dependent sulfide speciation is given as follows:

$$H_2S \overset{K_1}{\longleftrightarrow} HS^- + H^+; \quad K_1 = \frac{[HS^-][H^+]}{[H_2S]}; \quad pK_1 = 6.99 \quad (8)$$

$$HS^- \overset{K_2}{\longleftrightarrow} S^{2-} + H^+; \quad K_2 = \frac{[S^{2-}][H^+]}{[HS^-]}; \quad pK_1 = 12.9 \quad (9)$$

where the brackets represent dissolved concentrations, and pK is defined as the negative base-10 logarithm of the corresponding acid dissociation constant (K), i.e., $pK = -\log K$. Finally, the supersaturation criterion representing the thermodynamic onset of metal sulfide precipitation can be evaluated using the saturation ratio, Ω_{MeS}, defined as follows:

$$\Omega_{MeS} = \frac{IAP_{MeS}}{K_{sp,Mes}} = \frac{\{Me^{2+}\}\{S^{2-}\}}{K_{sp,Mes}} > 1 \quad (10)$$

where IAP_{MeS} is given by Equation 1 and $K_{sp,MeS}$ is given by Equation 2. Although thermodynamic activities are formally related to dissolved-species concentrations through activity coefficients, γ, or $\{\} = \gamma[]$, activities were approximated by measured dissolved concentrations in the present study by assuming unit activity coefficients ($\gamma \approx 1$). Consequently, the calculated saturation ratios should be regarded as approximate indicators of metal sulfide precipitation potential rather than rigorous thermodynamic saturation states.

Thermodynamically, $\Omega_{MeS} = 1$ represents equilibrium with respect to $MeS_{(s)}$, and $\Omega_{MeS} > 1$ indicates supersaturation favorable for precipitation. The reactions given by Equations 3–10 were used as the theoretical framework for CPS dosing and interpreting precipitation behavior, supersaturation development, and post-remediation stability in subsequent experiments.

The theoretical precipitation threshold (i.e., $\Omega_{MeS} = 1$) was evaluated via batch experiments by identifying the lowest or critical CPS dosage, $C_{CPS,Cri}$, at which the CPS-induced transition within the pH-versus-ORP domain coincided with the onset of substantial Cd and Zn precipitation. Although HS^- is typically the dominant reduced sulfide species from circumneutral to strongly alkaline conditions, metal sulfide precipitation is ultimately governed by the pH-dependent activity of S^{2-} and the total availability of reduced sulfur species, ΣS^{2-}. Therefore, CPS-induced immobilization is controlled by not only bulk aqueous condition as characterized by pH and ORP or redox potential (Eh), but also whether or not CPS addition generates sufficient reduced sulfur activity to increase Ω_{MeS} above the thermodynamic precipitation threshold and sustain $MeS_{(s)}$.

3. Materials and methods

3.1. Experimental materials

A commercially available calcium polysulfide solution (29% CPS; Lianyungang Yosoo Industrial Technique Co., China) was used as the sulfur-based remediation reagent in this study. Detailed physicochemical properties of the CPS solution, including those measured in this study, are summarized in Table S1. In brief, the CPS solution was an amber alkaline liquid comprising primarily calcium polysulfide species, generally represented as CaS_x (x = 2–7). The solution exhibited strong alkaline conditions ($11.2 \leq$ pH ≤ 11.6), a highly reducing ORP (< -240 mV), low dissolved oxygen (DO < 0.2 mg/L), and a density of 1.27–1.28 Mg/m^3, consistent with previously reported physicochemical properties of commercial CPS solutions [18,20].

3.2. Groundwater characterization and batch experiments

Groundwater samples for the CPS batch experiments were collected from three monitoring locations, designated GW−1, GW−2, and GW−3, within a multi-metal-contaminated area affected by historical smelting activities. Field parameters, including pH, ORP, DO, and electrical conductivity (EC), were measured immediately after sampling using calibrated portable probes (YSI Inc., USA: YSI 4110 for pH/ORP, YSI ProOBOD IDS for DO, and YSI Pro 30 for EC). Major cation concentrations were measured via inductively coupled plasma (ICP) with detection using optical emission spectroscopy (ICP-OES, iCAP PRO, Thermo Fisher Scientific, USA), whereas trace and heavy metal concentrations were measured using ICP with mass spectrometry detection (ICP-MS, iCAP RQ, Thermo Fisher Scientific, USA). Major anions were determined by ion chromatography using a 940 Professional ion chromatograph (IC Vario system, Metrohm, Switzerland). The chemical compositions of the groundwater samples are summarized in Table S2.

Marked differences in groundwater chemistry and dissolved metal concentrations were observed among the three sampling locations. Sample GW−1 comprised the lowest concentrations of 1.58 mg/L Cd and 113 mg/L Zn, whereas sample GW−2 comprised intermediate concentrations of 27.2 mg/L Cd and 1530 mg/L Zn. Sample GW−3 comprised the highest concentrations of 151 mg/L Cd and 6670 mg/L Zn, including substantially elevated concentrations of Mn, Mg, sulfate (SO_4^{2-}), and ionic strength (I) relative to the other sampling locations. Thus, these groundwater samples represented a broad range of Cd and Zn concentrations that provided for an evaluation of CPS-induced metal immobilization across marginally, moderately, and highly contaminated groundwater conditions.

Batch experiments were performed in triplicate using 50-mL polypropylene (PP) conical tubes at 25 ± 1 °C. In each reactor, 49 mL of contaminated groundwater was combined with 1 mL of CPS reagent solution prepared by diluting the commercial 29% (w/v) CPS stock solution with ultrapure water (EC < 0.5 mS/m). Site-specific CPS dosage ranges were selected based on preliminary tests and previously reported CPS-to-metal mass ratios [19–23], resulting in final CPS concentrations (v/v) of 0.0001–0.12%, 0.005–1.5%, and 0.001–10% for GW−1, GW−2, and GW−3, respectively. For each groundwater sample, $C_{CPS,Cri}$ was assigned as the lowest CPS dosage that induced rapid pH increase and ORP decrease coinciding with the onset of substantial Cd and Zn removal, and $C_{CPS,Opt}$ ($> C_{CPS,Cri}$) was assigned as the lowest CPS dosage that achieved near-maximum Cd and Zn removal without substantial additional improvement observed at higher CPS dosages. When $C_{CPS,Cri}$ and $C_{CPS,Opt}$ occurred within the same tested dosage range, the critical transition and operational optimum were not resolved further within the experimental dosage resolution.

After CPS addition, the sealed batch reactors were placed on a

horizontal orbital shaker and agitated at 130 rpm for 24 h to promote CPS dispersion/dissociation, sulfur-speciation reactions, and metal sulfide precipitation. The reactors then remained undisturbed for 24 h to allow quiescent settling. The supernatants subsequently were filtered through 0.45-μm hydrophilic PP membranes and analyzed for physicochemical parameters and residual dissolved metal concentrations (see Figs. S2 and S3).

3.3. Characterization of precipitates

Following batch experiments, the supernatants were decanted and the recovered solids were dried at 45 °C for 72 h prior to characterization. Crystalline phases were identified using X-ray diffraction (XRD; SmartLab, Rigaku, Japan), and surface chemical states were analyzed using X-ray photoelectron spectroscopy (XPS; Thermo Fisher Scientific, USA), focusing on the Zn 2p, Cd 3d, and S 2p spectral regions. The morphology and elemental distribution of the precipitates were examined by scanning electron microscopy coupled with energy-dispersive X-ray spectroscopy (SEM-EDS; SU8230, Hitachi, Japan; AMETEK, USA). Furthermore, transmission electron microscopy coupled with energy-dispersive X-ray spectroscopy (TEM-EDS: HF5000, Hitachi, Japan; Ultim Max, Oxford, UK) was employed to determine the internal structure and elemental distribution within the crystalline precipitates of sample GW−2. High-energy EDS linear scanning was performed across selected particles to specifically elucidate the elemental configuration inside the spherical precipitates, which were identified as potential crystal nuclei. Collectively, these analyses were used to determine whether CPS dosing produced sulfide-associated Cd and Zn phases together with secondary mineral phases formed during precipitation.

3.4. Leaching and sequential extraction tests

The stability of CPS-induced precipitates was evaluated using modified aqua regia digestion [26] and modified Tessier sequential extraction procedure [27]. Precipitates recovered from the three groundwater samples were digested with aqua regia (HCl:HNO_3 = 3:1 v/v) under microwave-assisted conditions at 95 °C for 2 h. Because aqua regia digestion does not fully decompose silicate-bound metal phases, the extracted metal mass was interpreted as the pseudo-total, aqua-regia-extractable fraction. Therefore, dissolution of metal sulfides during aqua regia processing was considered an operational oxidative extraction process involving oxidation and solubilization of sulfide-associated metals rather than a stoichiometrically defined elementary reaction as follows:

$$MeS_{(s)} + OAM \rightarrow Me^{2+}_{(aq)} + S^0 \Big/ SO_4^{2-} + DMC \quad (11)$$

where OAM represents oxidizing acid mixtures (e.g., HCl-HNO_3) and DMC represents dissolved metal complexes (e.g., $CdCl^+$, $CdCl_2$, $ZnCl^+$, $ZnCl_2$).

A modified five-step Tessier-type sequential extraction procedure [27] was performed subsequently to evaluate the operational distribution of Cd and Zn among exchangeable (F1), carbonate-bound (F2), Fe/Mn oxide-bound (F3), oxidizable organic matter/sulfide-associated (F4), and residual (F5) fractions. This procedure was applied as an operational tool to compare the relative extractability and chemical stability of CPS-derived precipitates based on different initial metal concentrations. Because these fractions are reagent-defined rather than mineral-specific, F4 may include metal sulfides, organic-associated metals, and other reduced sulfur-bearing phases, whereas F5 represents metals released only during the final residual digestion. Therefore, aqua-regia digestion and sequential extraction address different operational endpoints and were not interpreted as directly equivalent stability tests. The Cd and Zn concentrations in all extracts were quantified by ICP-OES.

4. Results and discussions

4.1. Geochemical transition and sulfide precipitation thresholds

The addition of CPS to the contaminated groundwater induced a pronounced transition from acidic, oxidizing conditions toward more alkaline and reducing conditions favorable for sulfide-mediated precipitation. As shown by the Eh–pH trajectories in Fig. 1, the untreated groundwater samples initially were positioned within dissolved Cd^{2+}/Zn^{2+} stability fields, whereas CPS-treated samples transitioned toward geochemical conditions that were favorable for $CdS_{(s)}$ and $ZnS_{(s)}$ formation. This transition is consistent with CPS hydrolysis and sulfur-speciation reactions generating reduced sulfur species, including polysulfides, HS^-/H_2S, and trace S^{2-}, that can react with dissolved Me^{2+} to form sparingly soluble metal sulfide precipitates [12,16–23,25,28].

Accordingly, Fig. 1 should be interpreted as a conceptual geochemical trajectory diagram illustrating the transition from dissolved-metal conditions toward sulfide-favoring conditions, rather than as a fully quantitative Pourbaix diagram. Specifically, thermodynamic phase boundaries were not calculated since dissolved sulfur activities, ionic-strength corrections, and conversion of measured ORP values to thermodynamic Eh were not fully incorporated in Fig. 1. Nevertheless, the observed transitions provide useful mechanistic insight into the geochemical evolution induced by CPS addition and demonstrate the associated shift toward conditions favorable for sulfide-mediated Cd and Zn immobilization.

However, transition into a sulfide-favoring Eh–pH domain does not necessarily guarantee measurable $MeS_{(s)}$ precipitation, because mineral formation requires that $IAP_{MeS} > K_{sp,MeS}$ for the target $MeS_{(s)}$. Therefore, $C_{CPS,Cri}$ should be interpreted as an operational rather than absolute precipitation-onset threshold representing the lowest CPS dosage at which the CPS-induced geochemical transition, indicated by a rapid increase in pH and decrease in ORP, coincided with the onset of substantial Cd and Zn removal via sulfide precipitation. For CPS dosing lower than this threshold, CPS addition may still alter pH and ORP, but the availability of reduced sulfur may remain insufficient to sustain $CdS_{(s)}$ and $ZnS_{(s)}$ precipitation. Once $C_{CPS,Cri}$ is exceeded, supersaturation increases, the nucleation barrier decreases, and rapid metal sulfide precipitation becomes both thermodynamically and kinetically favorable.

As a result, $C_{CPS,Opt}$ ($\geq C_{CPS,Cri}$) is defined as the lowest CPS dosage at which Cd and Zn removal approaches a near-maximum plateau, such that further CPS addition produces only marginal additional removal while increasing the potential for excessive increase in pH and decrease in ORP, residual sulfur accumulation, and secondary precipitate formation. Thus, in this study, $C_{CPS,Cri}$ represents the apparent precipitation-onset threshold, whereas $C_{CPS,Opt}$ represents the practical, minimum operational dosing such that additional CPS produces only marginal improvement in metal removal efficiency. This interpretation is consistent with the inflection points observed in residual Cd and Zn concentrations shown in Fig. 2, where metal removal increased sharply as CPS dosage exceeded $C_{CPS,Cri}$ and then approached asymptotically a limiting plateau near $C_{CPS,Opt}$.

Quantitatively, the $C_{CPS,Cri}$ values for Cd were 24, 40, and 220 mg/L for GW−1, GW−2, and GW−3, respectively, and coincided with the corresponding $C_{CPS,Opt}$ values within the tested dosage resolution. For Zn, the respective $C_{CPS,Cri}$ values were 286, 1970, and 1.00×10^4 mg/L, whereas the respective $C_{CPS,Opt}$ values were higher at 580, 3860, and 16,500 mg/L. The consistently lower thresholds for Cd indicate that substantial Cd removal began at lower CPS dosages, whereas Zn required additional reduced-sulfur capacity to achieve near-maximum removal. Because these thresholds were identified from discrete experimental dosages, these results should be interpreted as operational rather than exact thermodynamic transition points. The significant separations between $C_{CPS,Cri}$ values for Cd and Zn also suggest a potential selective precipitation window. For GW−2 and GW−3, Cd removal

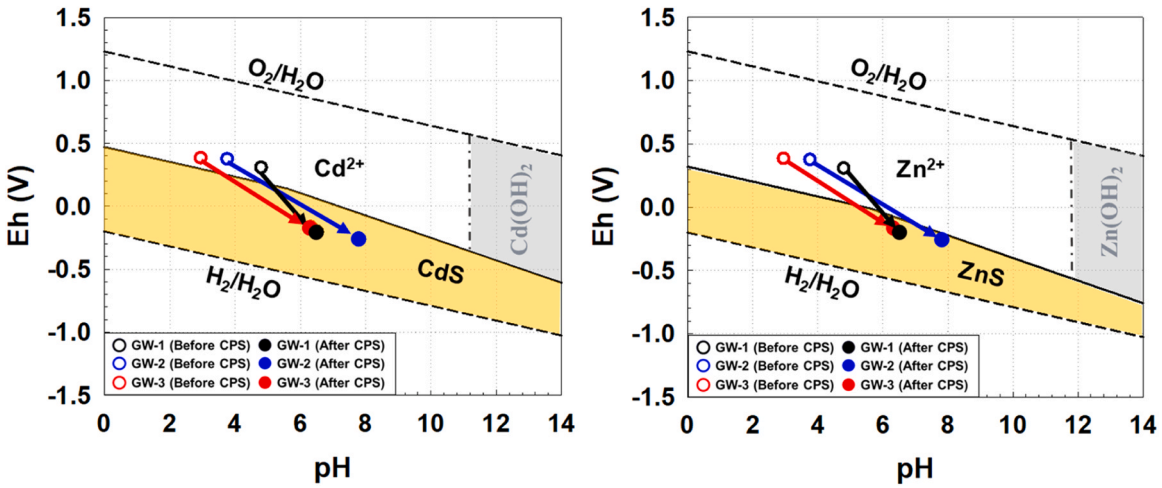

Fig. 1. Approximate Pourbaix diagrams of pH versus redox potential (Eh) for Cd and Zn showing the measured geochemical trends from before to after calcium polysulfide dosing in batch reactors. [Notes: Experimental conditions transitioned from acidic, oxidizing groundwater toward more alkaline and reducing sulfide-favoring conditions, consistent with the shift from dissolved Cd^{2+}/Zn^{2+} to $CdS_{(s)}$/$ZnS_{(s)}$-stability fields. Water-stability boundaries are shown for reference. Mineral boundaries are schematic and intended only to illustrate the direction of geochemical evolution after CPS dosing.].

began at substantially lower CPS dosages than Zn removal. However, the exact boundaries of this window cannot be resolved because the tested dosages were designed to identify co-immobilization thresholds rather than selective separation conditions. Further titration experiments using closely spaced sub-critical CPS dosages are required to verify preferential Cd precipitation before substantial Zn removal.

The observed threshold behavior was metal-specific. For example, Cd was removed at lower CPS dosages and across narrower transition intervals than Zn, reflecting the lower solubility and greater precipitation tendency of $CdS_{(s)}$ relative to $ZnS_{(s)}$. In contrast, Zn immobilization required greater reduced sulfur availability and higher supersaturation conditions, resulting in broader removal transitions, particularly under the higher concentration conditions at the locations of GW−2 and GW−3. These differences indicate that effective CPS dosing cannot be determined solely from total dissolved metal concentration or bulk pH adjustment. Instead, design of effective CPS dosing must account for metal-specific sulfide solubility, reduced sulfur speciation, and competing geochemical demand. In sulfate-rich, multi-metal-contaminated groundwater, a portion of the injected CPS also may be consumed by background oxidant demand such as Fe/Mn redox cycling, secondary sulfur transformations, and Ca-bearing precipitate formation, thereby reducing the fraction of CPS available for targeted $CdS_{(s)}$ and $ZnS_{(s)}$ precipitation [19–23].

4.2. Site-specific geochemical response and concentration-dependent CPS dosing framework

The coupled geochemical responses and residual metal concentrations as a function of CPS dosage for the three groundwater samples are shown in Fig. 2. Across all samples, CPS dosing transitioned groundwater towards conditions that were more favorable for sulfide-mediated metal precipitation, as indicated by increasing pH and decreasing ORP. However, DO and EC responses were dependent on the groundwater sample and partly non-monotonic, reflecting the combined effects of sulfide addition, oxygen consumption, precipitation reactions, ionic-strength changes, and matrix buffering. These observations indicate that CPS-induced transitions should be interpreted using the coupled responses of pH, ORP, DO, EC, and residual metal concentrations rather than any single geochemical parameter.

Relatively low CPS dosages were required for remediation of the groundwater sample with low metal concentrations (GW−1), resulting in relatively modest changes in pH, ORP, DO, and EC. This result suggests that added CPS was consumed primarily by background oxidant demand and competing matrix reactions and was insufficient to establish persistent sulfide-rich conditions. Near the critical dosage ($C_{CPS,Crt}$), ORP and DO decreased and pH began to increase, marking the onset of reducing and sulfide-favoring conditions. The residual metal profiles indicate that Cd decreased rapidly and approached near-complete removal at lower CPS dosages, whereas Zn required a slightly higher dosage and exhibited a broader removal transition. Manganese (Mn) decreased primarily near or above the optimal dosage range ($C_{CPS,Opt}$), while magnesium (Mg) remained comparatively persistent, indicating that Mg immobilization was limited under the tested conditions and was not controlled primarily by stable sulfide precipitation.

For GW−2, the geochemical transition and metal removal occurred over a broader CPS dosage interval. Because the initial Cd and Zn concentrations were substantially higher than those for GW−1, greater CPS addition was required before a distinct decrease in ORP, increase in pH, and near-complete metal removal were achieved. Cadmium removal again occurred at lower CPS dosages than those for Zn removal, consistent with the greater thermodynamic favorability for $CdS_{(s)}$ formation. In contrast, Zn removal required a wider dosage interval and higher reduced-sulfur availability, reflecting the greater Zn mass loading and the need to generate sufficient supersaturation for sustained $ZnS_{(s)}$ precipitation. The Mn and Mg responded primarily at higher CPS dosages, suggesting that removal was associated with stronger perturbation of bulk groundwater chemistry rather than selective precipitation under the initial Cd/Zn sulfide-precipitation threshold conditions.

The greatest CPS dosage required to achieve comparable transformation among the three groundwater samples was observed for GW−3, the most contaminated and highest ionic-strength groundwater. In the lower CPS dosage region, pH and ORP changed only gradually, indicating that much of the added CPS was consumed initially by the high dissolved metal mass loading, oxidant demand, and competing matrix constituents. A pronounced transition occurred only at higher CPS dosages, where ORP decreased markedly and pH increased sharply. Cadmium reached the removal threshold at lower CPS dosages than Zn, demonstrating distinct concentration-dependent precipitation responses between the two metals. Manganese decreased mainly under high CPS addition, whereas Mg remained relatively resistant to immobilization, further supporting the interpretation that CPS remediation selectively favored Cd and Zn sulfide precipitation over Mg removal.

Collectively, the batch results define three operational CPS dosages. In the sub-threshold dosages, CPS addition partially modified pH and ORP, but reduced sulfur availability was insufficient to sustain complete Cd and Zn precipitation, resulting in elevated residual metal

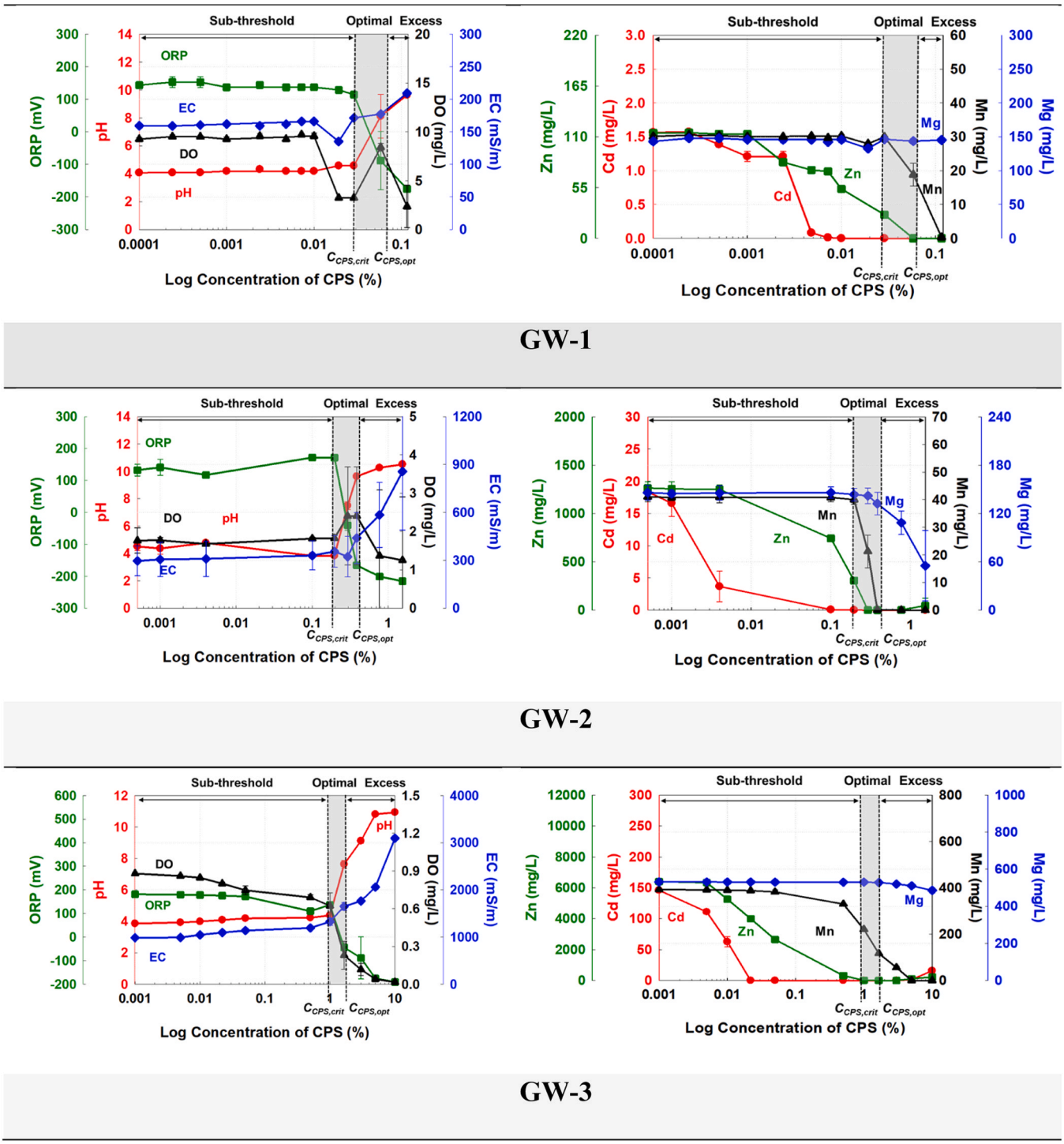

Fig. 2. Geochemical responses and aqueous metal removal as a function of calcium polysulfide (CPS) dosage for three groundwater samples (GW−1, GW−2, and GW−3) collected from different locations within the same smelting-impacted site. [Notes: Left panels show changes in oxidation-reduction potential (ORP), pH, dissolved oxygen (DO), and electrical conductivity (EC), whereas right panels show residual aqueous concentrations of Cd, Zn, Mn, and Mg. Shaded regions indicate the optimal (operational) CPS dosage ranges selected to achieve substantial Cd and Zn precipitation while minimizing excessive geochemical disturbance.].

concentrations and limited geochemical perturbation. For optimal dosages, CPS addition generated sufficient reduced sulfur activity to exceed the saturation threshold for $CdS_{(s)}$ and $ZnS_{(s)}$, i.e., $\Omega_{MeS} > 1$. Under this condition, substantial Cd and Zn removal was achieved within the experimental reaction period, without excessive increases in pH, EC, or an unnecessarily large decrease in ORP. In the excess-reagent region, further CPS dosing produced stronger geochemical perturbation but little additional Cd or Zn removal, indicating diminishing returns in remediation efficiency. Excess CPS may, therefore, be diverted into non-target pathways, including sulfur-speciation transitions, secondary sulfur-phase formation, reactions with competing matrix constituents, and Ca-bearing secondary precipitate formation.

The absolute $C_{CPS,Opt}$ values identified from Fig. 2 increased from samples GW−1 to GW−3, reflecting increasing initial metal concentrations and geochemical matrix demand. In contrast, when the dosage is normalized to the dissolved Cd and Zn mass, as shown in Fig. 3, the

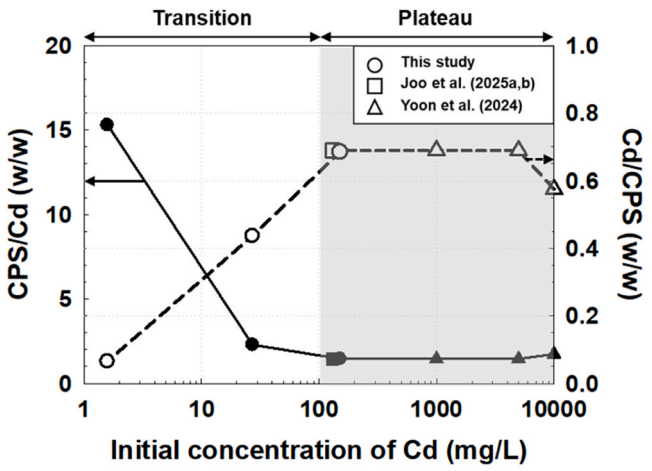

(a)

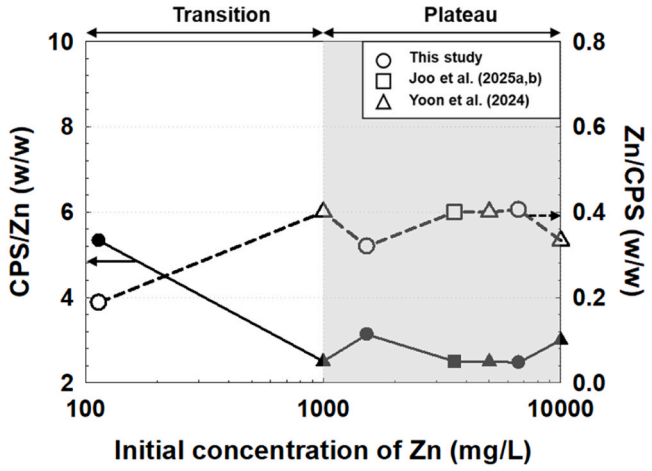

(b)

Fig. 3. Simplified dosage framework showing the relationship between optimal calcium polysulfide (CPS) dosage and initial dissolved metal concentration expressed as the required CPS/metal mass ratio (w/w): (a) Cd; (b) Zn.

required CPS-to-metal ratio decreased nonlinearly with increasing initial metal concentration. Specifically, the optimal CPS/Cd mass ratio decreased from 15.9 for GW−1 to 2.29 for GW−2 and 1.46 for GW−3, whereas the corresponding CPS/Zn ratio decreased from 5.33 for GW−1 to 3.13 for GW−2 and 2.47 for GW−3. Although the absolute CPS dosage increased with initial metal loading, the CPS requirement per unit metal mass decreased substantially. This trend is consistent with a proportionally greater influence of background oxidant demand and matrix reactions at low metal concentrations, whereas higher metal concentrations more readily promoted sulfide supersaturation.

Additionally, this trend indicates that groundwater contaminated with low concentrations of Cd and Zn requires disproportionately greater CPS addition per unit metal mass, because a substantial fraction of CPS is consumed by background oxidant demand, pH buffering, sulfur transformation, and competing matrix reactions before effective metal sulfide supersaturation is achieved. This behavior suggests a transition from a low-concentration regime, where background matrix demand and nucleation limitations dominate CPS utilization, to a high-concentration regime, where target-metal sulfide precipitation becomes more efficient because supersaturation is more readily achieved. Conceptually, the optimal CPS dosage can be expressed as follows:

$$C_{CPS,Opt} = f\left(C_{Me,Ini}, \Omega_{MeS}, K_{sp,MeS}, \text{matrix chemistry}\right) \quad (12)$$

While the absolute $C_{CPS,Opt}$ increased with increasing $C_{Me,Ini}$, the normalized CPS-to-metal ratio decreased nonlinearly with $C_{Me,Ini}$. This deviation from simple stoichiometric scaling likely indicates that CPS demand was not governed solely by Cd and Zn sulfide precipitation. Instead, an apparent site-specific baseline CPS demand likely was consumed by background oxidants, pH buffering reactions, sulfur-speciation transitions, and competing matrix reactions before sufficient reduced sulfur activity became available to drive supersaturation-dependent nucleation and growth of $MeS_{(s)}$ precipitates [19–23]. Consequently, the values of $C_{CPS,Cri}$ and $C_{CPS,Opt}$ should be regarded as matrix-specific dosing parameters that require site-specific calibration rather than universal stoichiometric constants.

Overall, a mechanistically based CPS dosing framework is established in Figs. 1–3. The direction of geochemical transition toward sulfide-favoring conditions is demonstrated in Fig. 1, the site-specific threshold and optimal dosage regions based on coupled geochemical response and residual metal removal are identified in Fig. 2, and these observations are translated into concentration-dependent CPS-to-metal scaling relationships in Fig. 3. This framework advances CPS remediation beyond empirical dosing by linking reagent demand to initial metal concentration, metal-specific sulfide solubility, supersaturation development, and geochemical matrix demand (see Equation 12). For field-scale application, this distinction is critical because CPS overdosing may increase pH and EC, and cause unnecessary ORP depression without proportional removal benefits, whereas CPS underdosing may fail to exceed the values of $C_{CPS,Opt}$ required for sustained Cd and Zn immobilization.

4.3. Mineralogical and surface chemical characterization of CPS-derived precipitates

The combined results of the mineralogical and surface chemical analyses using SEM-EDS, TEM-EDS, XRD, and XPS indicate that CPS injection produced a chemically heterogeneous precipitate assemblage comprising metal-sulfide-associated phases, Ca-bearing sulfate minerals, and secondary sulfur species (Fig. 4, S4, and S5). This mixed assemblage reflects the simultaneous occurrence of metal sulfidation, Ca-sulfate precipitation, and transformation of CPS-derived reduced sulfur species under sulfate-rich, multi-metal-contaminated groundwater conditions.

Mapping by SEM-EDS revealed precipitate-enriched domains in which Zn and S were strongly co-localized, supporting the formation of solid phases with Zn-S. Calcium also was spatially associated with several precipitate regions, suggesting the coexistence of Ca-bearing secondary minerals, such as gypsum ($CaSO_4 \bullet 2H_2O$). However, since EDS provides elemental distributions rather than crystallographic information, Ca-S co-localization alone should not be interpreted as direct proof of gypsum formation. Instead, the SEM-EDS results indicate that CPS-derived precipitates were not comprised exclusively of metal sulfides, but rather included mixed sulfide- and sulfate-associated phases.

This interpretation is consistent with the sulfate-rich groundwater matrix, where dissolved sulfate can promote Ca-sulfate precipitation following CPS dissociation and Ca^{2+} release [21–23]. Such secondary Ca-bearing precipitates may influence precipitate texture, spatial continuity, pore-scale accumulation, and apparent reagent efficiency. Therefore, SEM-EDS results should be interpreted together with XRD and XPS analyses to distinguish between elemental association, mineralogical identity, and surface chemical binding states. In this context, the co-occurrence of Zn-S-rich domains, Ca-S-bearing regions, and sulfur-bearing secondary phases supports a heterogeneous immobilization mechanism in which Cd and Zn sequestration is driven primarily by sulfide precipitation, while Ca-sulfate formation represents an important competing or accompanying reaction pathway [21–23].

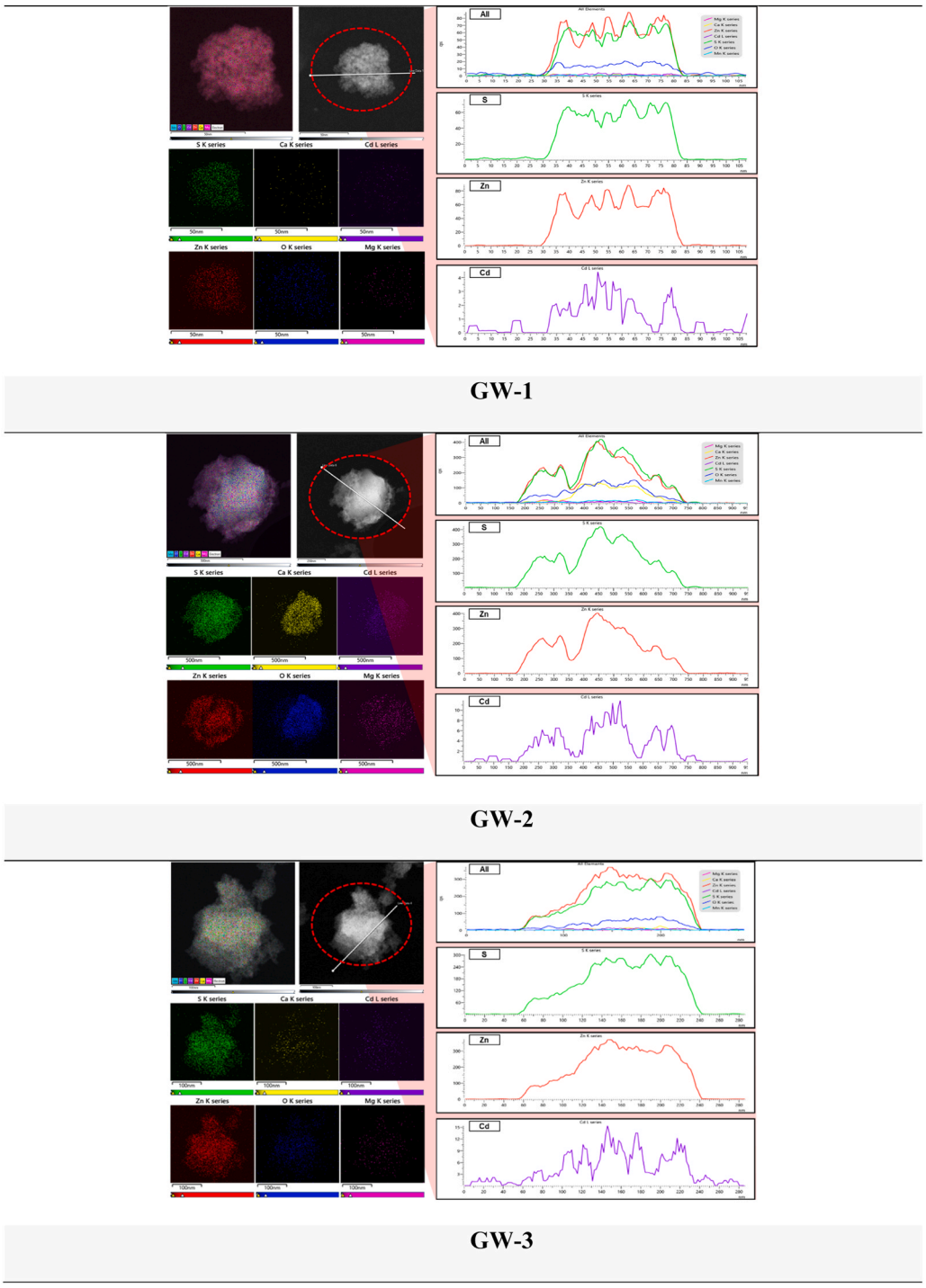

Fig. 4. TEM–EDS elemental mapping of three groundwater samples (GW−1, GW−2, and GW−3) confirming nanoscale spatial association among Cd, Zn, S, and Ca, consistent with coexistence of Zn-bearing sulfide-associated precipitates and Ca-bearing secondary phases.

The TEM-EDS analysis provided higher-resolution evidence of nanoscale precipitate formation (see Fig. 4). The TEM images revealed aggregated, electron-dense particles with irregular clustered morphologies, consistent with rapid precipitation under locally reducing and sulfide-rich conditions. Elemental mapping further confirmed spatial co-localization of Ca, S, Cd and Zn at the nanoscale, supporting the coexistence of Zn-bearing sulfide-associated particles and Ca-bearing secondary precipitates. In contrast, the Cd signal was insufficient for reliable spatial localization, possibly because of the relatively low abundance and the nanoscale or poor crystalline nature of the Cd-bearing phases. Because TEM-EDS provides elemental rather than crystallographic information, these observations do not independently confirm the formation of crystalline $CdS_{(s)}$. Instead, Cd immobilization through sulfide-associated precipitation is supported by the collective evidence based on aqueous removal, mass balance, sequential extraction, and XPS, but remains partially inferential in the absence of direct crystallographic identification. More definitive confirmation would require High-Resolution Transmission Electron Microscopy/Selected Area Electron Diffraction, or analysis of Cd-enriched precipitates generated under selectively controlled dosing conditions.

The XPS results provided surface-sensitive evidence for metal-sulfur bonding and sulfur speciation within the CPS-derived precipitates. The

Zn 2p and Cd 3d spectra were consistent with Zn- and Cd-bearing sulfide coordination environments, supporting the interpretation that both metals were immobilized, at least partially, through sulfide-associated bonding. Deconvolution of the S 2p spectra indicated multiple sulfur species, including S^{2-} (161.8 eV), S^0 (163.7 eV), and SO_4^{2-} (168.5 eV). The coexistence of reduced, intermediate, and oxidized sulfur species demonstrates that CPS remediation generated a chemically heterogeneous sulfur assemblage. The sulfide component supports Cd and Zn sulfidation, whereas S^0 and SO_4^{2-} components indicate concurrent sulfur transformation and secondary mineral formation. Therefore, the XPS results strengthen the interpretation of sulfide-associated immobilization, particularly for Cd, whose crystalline sulfide phase was not clearly detected by XRD.

The XRD analysis identified gypsum, sphalerite-type $ZnS_{(s)}$, and S^0 as

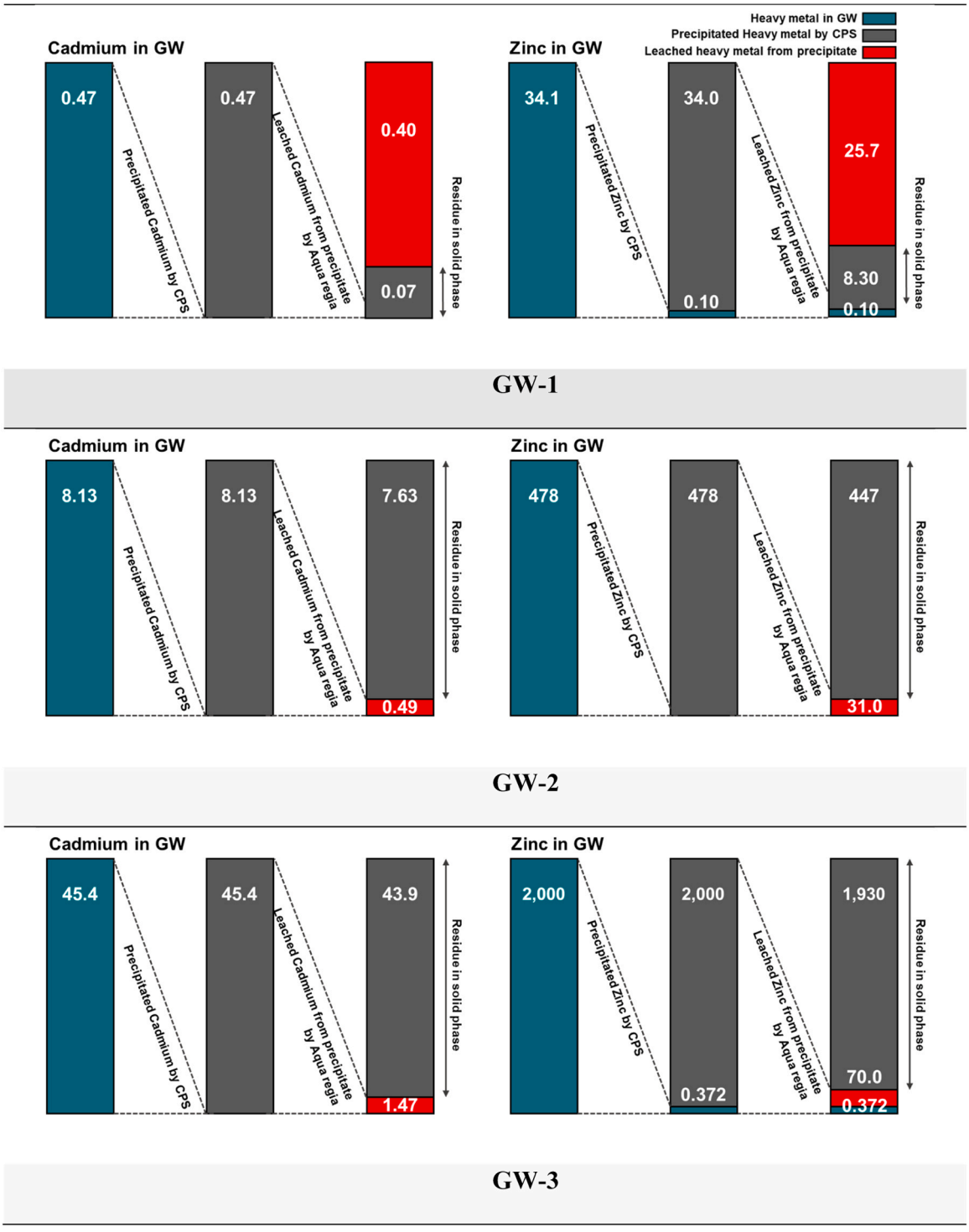

Fig. 5. Mass-balance comparison in milligrams of Cd and Zn in three groundwater samples (GW−1, GW−2, and GW−3) before calcium polysulfide (CPS) dosing, after CPS-induced precipitation, and after subsequent acid extraction. [Notes: Teal bars represent dissolved metals initially present in GW, gray bars represent the total mass transferred to CPS-derived precipitates, and red bars indicate the fraction re-extracted by acid treatment. The remaining gray fraction represents the acid-non-extractable residual metal retained in solid-associated phases.].

crystalline phases in the CPS-derived precipitates. The detection of crystalline $ZnS_{(s)}$ provides direct mineralogical evidence that Zn immobilization occurred, at least partially, through sulfide precipitation. The presence of gypsum confirms that Ca released from CPS dissociation reacted with sulfate in the groundwater, indicating that a portion of the injected reagent participated in non-target secondary mineral formation. Elemental sulfur likely reflects partial oxidation, disproportionation, or transformation of reduced sulfur species during and after CPS reaction. In contrast, $CdS_{(s)}$ was not clearly resolved in the XRD patterns. This lack of resolution should not be interpreted as evidence that $CdS_{(s)}$ did not form, because Cd-bearing sulfide phases may have been present at low abundance, nanoscale, poorly crystalline, or partially amorphous forms that were below the detection limit of XRD. Thus, the XRD results confirm the presence of crystalline $ZnS_{(s)}$, gypsum, and elemental sulfur, but do not exclude the coexistence of less crystalline Cd-bearing or Zn-bearing secondary sulfide phases.

Overall, the SEM-EDS, TEM-EDS, XPS, and XRD results provide multiscale evidence that CPS remediation immobilized Cd and Zn predominantly through sulfide-associated precipitation, while also generating gypsum and S^0 as secondary products. These secondary phases reflect matrix-dependent secondary reactions arising from the sulfate-rich groundwater and CPS-derived calcium and sulfur species. Collectively, the characterization results support the proposed mechanistic framework described by Equation (12), indicating that CPS-induced metal immobilization is controlled by not only transitions in pH and ORP, but also the extent of supersaturation, nucleation, sulfur speciation, and site-specific groundwater geochemistry.

4.4. Operational extractability and fractionation of CPS-derived precipitates

The mass-balance comparison before CPS remediation, after CPS-induced precipitation, and following acid extraction demonstrates that most dissolved Cd and Zn were retained in CPS-derived solid phases (see Fig. 5). The acid-extractable fraction was low relative to the total precipitated fraction, indicating that a large portion of immobilized Cd and Zn remained associated with the solid phase after extraction. This difference between the precipitated mass and the acid-extractable mass was more pronounced at higher initial metal concentrations. These results suggest that precipitates formed under metal-rich conditions were less susceptible to acid extraction, possibly due to more complete sulfide incorporation, enhanced particle aggregation, and/or greater crystallinity during CPS-induced precipitation. Higher supersaturation under elevated metal loading also may have promoted faster nucleation and growth of sulfide-associated phases, thereby reducing apparent extractability.

The Sankey mass-flow analysis further supports the selective immobilization of Cd and Zn by CPS remediation (see Fig. 6). Both Cd and Zn were partitioned predominantly into CPS-derived precipitates and residual solid-associated fractions, whereas Mn and Mg remained largely in the aqueous phase. This contrast is consistent with the stronger chalcophile behavior and lower sulfide solubility of Cd and Zn compared with Mg and Mn. The relatively minimal, leached fractions of Cd and Zn indicate that the CPS-derived precipitates were resistant to dissolution during the applied extraction step. However, this result should not be interpreted as definitive evidence of permanent immobilization. Under field conditions, changes in pH, Eh, DO, microbial sulfur cycling, or carbonate/sulfate chemistry could alter the stability of metal sulfide phases and potentially induce partial remobilization.

The relationship between extraction efficiency and initial metal concentration is shown in Fig. 7, where extraction efficiency is defined as the fraction of the precipitated metal that was re-extracted during acid dissolution. The Cd extraction efficiency decreased from 84.0% for GW−1 to 6.04% for GW−2 and 3.24% for GW−3, whereas the Zn extraction efficiency decreased from 75.5% for GW−1 to 6.66% for GW−2 and 3.48% for GW−3. Thus, precipitates formed in the higher-

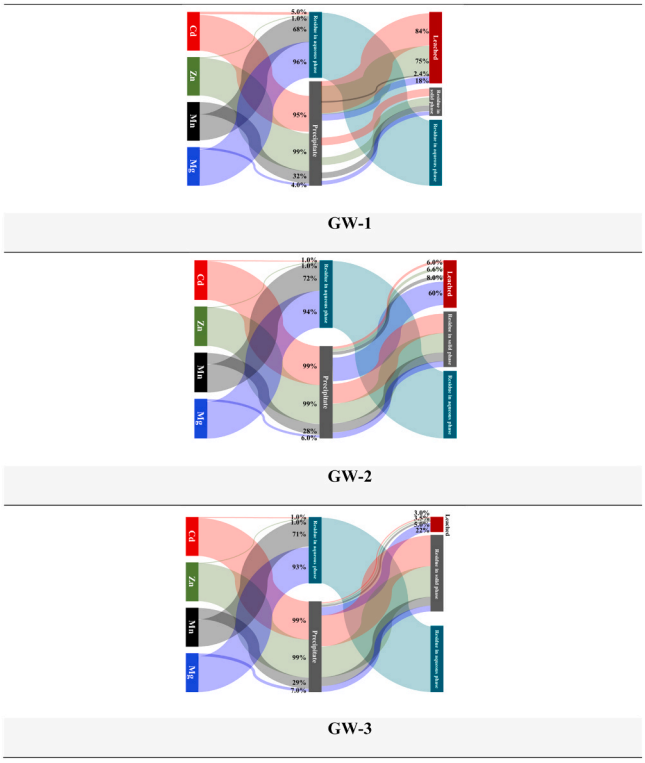

Fig. 6. Sankey mass-flow diagrams showing partitioning of Cd, Zn, Mn, and Mg during calcium polysulfide (CPS) treatment for three groundwater samples (GW−1, GW−2, and GW−3) collected from different locations within the same smelting-impacted site. [Notes: Percentages represent fractions relative to the initial dissolved metal mass. Metals were partitioned among residual aqueous phases, CPS-derived precipitates, acid-leached fractions, and residual solid-associated fractions.].

concentration groundwaters retained more than 93.0% of the precipitated Cd and Zn after acid extraction, whereas those formed in GW−1 were considerably more susceptible to dissolution. This pronounced concentration dependency supports the proposed relationship between initial metal loading and precipitate extractability, although the acid-extraction results should not be interpreted as direct predictions of long-term stability under field oxidation conditions.

The extraction efficiency decreased systematically with increasing initial Cd and Zn concentrations, indicating that precipitates formed at higher $C_{Me,Ini}$ were less acid-extractable than those formed under lower-concentration conditions. This inverse concentration-extractability trend is consistent with the proposed concentration-dependent precipitation framework. At higher $C_{Me,Ini}$, once sufficient reduced sulfur is supplied, greater dissolved metal activity can produce higher supersaturation with respect to $CdS_{(s)}$ and $ZnS_{(s)}$, thereby promoting rapid nucleation, particle growth, aggregation, and formation of less extractable sulfide-rich solids. Conversely, lower-concentration systems may remain closer to the critical supersaturation threshold, leading to less complete sulfide incorporation, smaller or more poorly crystalline particles, and slightly greater extractability. Although this mechanistic interpretation is plausible and consistent with the characterization results, this interpretation should be regarded as inferential unless supported by direct particle-size analysis, crystallinity quantification, or phase-specific mass balance.

Sequential extraction provided additional evidence that CPS remediation transformed Cd and Zn into less labile geochemical forms (see Fig. 8). Most Cd and Zn were associated with sulfide-bound/oxidizable and residual fractions, whereas exchangeable, carbonate-bound, and oxide-bound fractions were comparatively minor. More specifically, the low fractions of exchangeable (F1), carbonate-bound (F2), and Fe/Mn

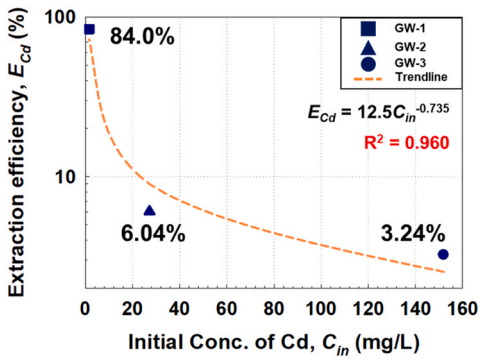

(a)

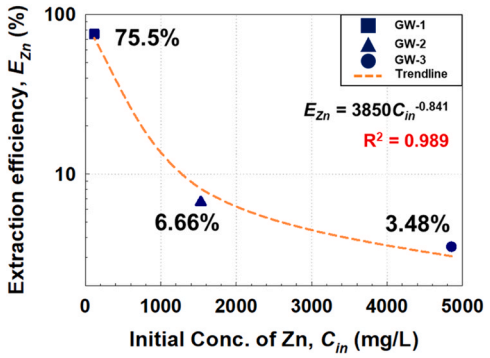

(b)

Fig. 7. Relationship between extraction efficiency and initial metal concentration: (a) Cd; (b) Zn. [Note: Extraction efficiency (E) was defined as the fraction of precipitated metal re-extracted during acid dissolution relative to the total precipitated metal mass.].

oxide-bound Cd and Zn (F3) indicate that only a limited fractions of the immobilized metals remained susceptible to rapid release through ion exchange, acidification, or reductive dissolution of oxide phases. In contrast, the predominant fractions associated with the sulfide-bound/oxidizable (F4) and residual (F5) indicate substantially reduced short-term mobility following CPS treatment.

Based on the collective results shown in Figs. 5–8, CPS remediation immobilized Cd and Zn primarily through formation of low-extractability solid phases, with apparent extractability decreasing as $C_{Me,Ini}$ increased. The low acid-extractable fractions, preferential partitioning of Cd and Zn into sulfide-associated and residual pools, and limited immobilization of Mn and Mg indicate that CPS-induced metal removal was governed primarily by precipitation and solid-phase transformation rather than reversible adsorption. The concentration-dependent decrease in extraction efficiency suggests further that supersaturation-driven precipitation influenced not only metal removal efficiency but also post-remediation extractability and apparent stability of CPS-derived precipitates. However, further evaluation of long-term field persistence of CPS-derived precipitates should be undertaken with respect to fluctuating pH-Eh conditions, oxidative aging, and repeated wetting-drying or groundwater-flow regimes, as well as microbially mediated sulfur transformations that may alter sulfide stability and metal mobility over time.

4.5. Supersaturation-driven nucleation and growth mechanisms of CPS-induced metal sulfides

The concentration-dependent differences in metal removal, precipitate extractability, and solid-phase partitioning can be interpreted using a supersaturation-controlled precipitation framework. Following CPS dosing, reduced sulfur species generated from CPS increase the saturation state of groundwater with respect to $CdS_{(s)}$ and $ZnS_{(s)}$. Metal sulfide precipitation becomes thermodynamically favorable when the saturation ratio, Ω_{MeS}, exceeds unity. However, thermodynamic favorability alone does not ensure immediate or complete precipitation because mineral formation also depends on nucleation barriers, particle growth, aggregation, and competing matrix reactions.

Classical nucleation theory provides a useful qualitative basis for interpreting the observed concentration-dependent precipitation behavior. This conceptual interpretation agrees with previous crystallization studies showing that increasing supersaturation accelerates nucleation, particle aggregation, and crystal growth, resulting in less soluble and more stable precipitates [13,14]. The present study experimentally links these crystallization concepts to concentration-dependent CPS dosing and heavy-metal immobilization in groundwater. In simplified form, the critical free-energy barrier for nucleation, ΔG^*, is inversely related to the square of the logarithm of supersaturation as follows:

$$\Delta G^* \propto \frac{\sigma^3}{(\ln \Omega)^2} \tag{13}$$

where σ is the interfacial energy between the nucleus and solution, and Ω is the saturation ratio of the relevant $MeS_{(s)}$. This relationship indicates that even moderate increases in supersaturation can substantially reduce the nucleation barrier, thereby favoring the formation of $CdS_{(s)}$ and $ZnS_{(s)}$ nuclei. Because nucleation rates, induction times, interfacial energies, and particle-size evolution were not directly measured in this study, Equation 13 should be interpreted as a conceptual framework for interpreting the observed concentration-dependent precipitation behavior.

The proposed crystallization pathway is summarized conceptually in Fig. 9. Under high initial metal concentration conditions, elevated dissolved metal concentrations allow the system to reach higher supersaturation once sufficient CPS-derived reduced sulfur becomes available. These high- Ω conditions reduce the nucleation barrier and promote rapid formation of metal sulfide nuclei. Subsequent particle growth, aggregation, and possible structural ordering then may generate sulfide-rich precipitates with lower acid extractability. This interpretation is corroborated by complementary multiscale evidence (see Fig. 4, S4, and S5), including Zn–S-bearing domains observed by SEM-EDS and TEM-EDS, sulfide sulfur identified by XPS, and crystalline ZnS detected by XRD. These observations, together with the mass-balance and sequential extraction results (see Figs. 5–8), demonstrate that a substantial fraction of Cd and Zn was retained in low-extractability solid-phase forms following CPS remediation.

In contrast, under low initial metal concentration conditions, supersaturation may develop more gradually and remain closer to the critical precipitation threshold. Under such near-threshold conditions, nucleation density may be lower, and precipitates may be more heterogeneous, less crystalline, or less completely incorporated into sulfide-rich phases. These solids may include poorly ordered metal-sulfur precipitates, surface-associated metal sulfide clusters, and/or mixed sulfide-sulfate assemblages. Such phases are expected to exhibit greater susceptibility to acid extraction than precipitates formed under higher supersaturation conditions. This conceptual framework is consistent with the observed inverse relationship between extraction efficiency and initial metal concentration (see Fig. 7), as well as the sequential-extraction results (see Fig. 8) indicating that Cd and Zn were predominantly partitioned into sulfide-associated and residual fractions, with comparatively greater extractability under lower-concentration conditions.

Post-nucleation processes such as particle aggregation, recrystallization, and Ostwald ripening may further reduce extractability by

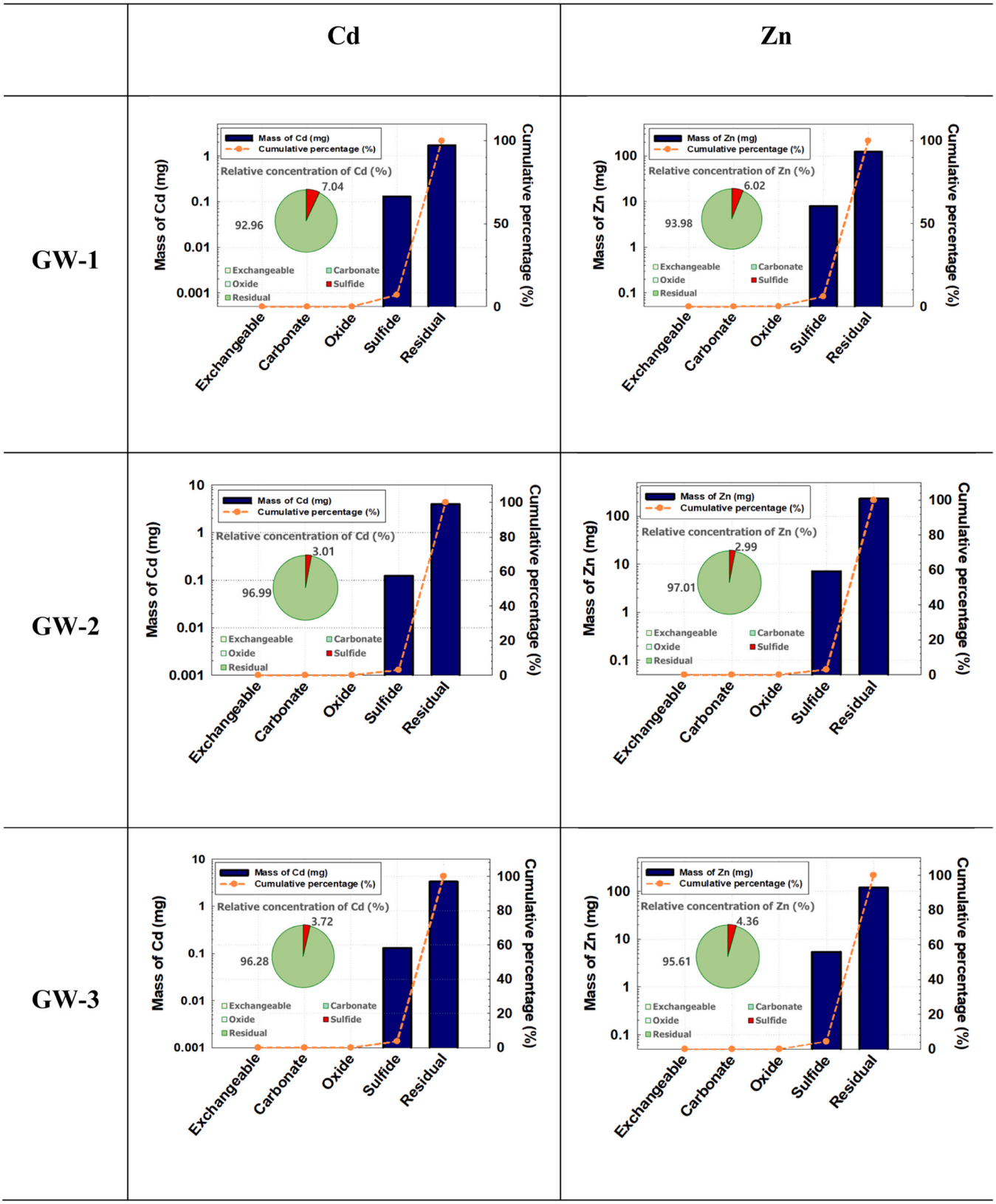

Fig. 8. Sequential-extraction results for Cd and Zn associated with calcium polysulfide (CPS)-derived precipitates from three groundwater samples (GW−1, GW−2, and GW−3) collected from different locations within the same smelting-impacted site. [Note: Bar plots show absolute and cumulative metal distributions among exchangeable, carbonate-bound, oxide-bound, sulfide-associated/oxidizable, and residual fractions, whereas pie charts show relative proportions.].

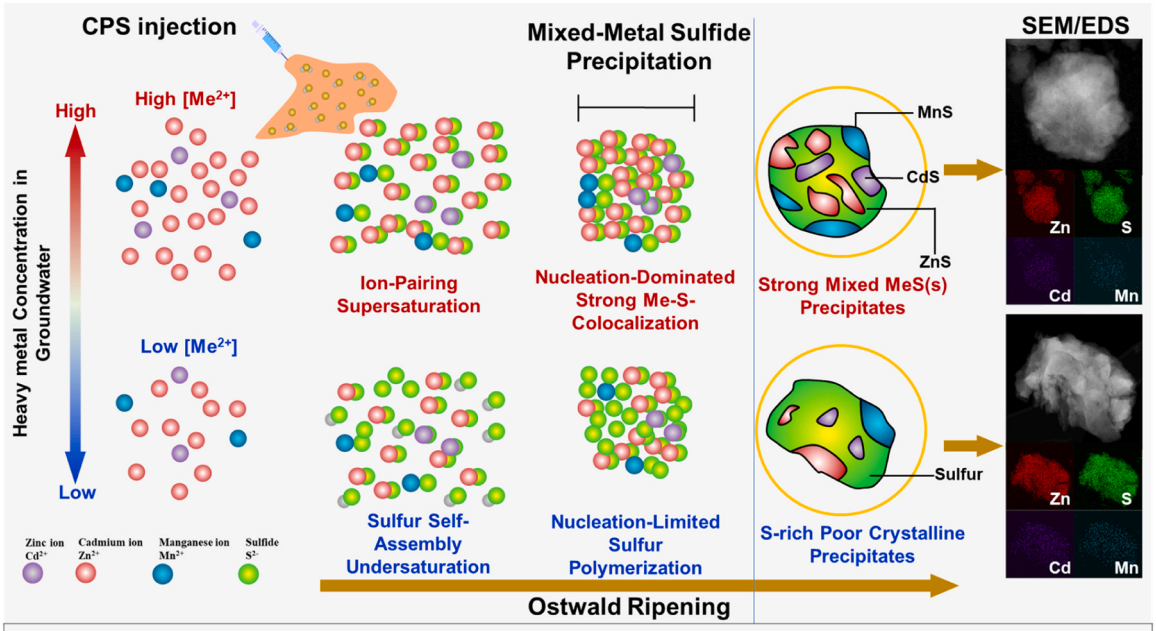

	High Me^{2+} Concentration	Low Me^{2+} Concentration
Supersaturation	Very High	Lower than Threshold
Nucleation Rate	Rapid	Slow
Crystallinity	Strong Me-S-Colocalization	S-rich Poor Crystalline
Sulfur Fate	Consumed in $MeS_{(s)}$	Polymerized/Oxidized
Metal Leaching	Low from Tight Lattice	High from Weak Matrix

Fig. 9. Conceptual supersaturation-controlled crystallization pathways for calcium polysulfide (CPS)-induced metal sulfide precipitation under contrasting concentration regimes.

transforming initially small or poorly ordered particles into larger, more stable, and less reactive solid phases. However, direct time-resolved evidence for these processes was not obtained in this study. Therefore, these processes should be regarded as plausible post-precipitation mechanisms rather than directly verified pathways. A more conservative interpretation is that increasing $C_{Me,Ini}$ enhanced supersaturation after CPS addition, thereby promoting more extensive nucleation, particle aggregation, and formation of less extractable sulfide-associated solids.

Overall, CPS-induced immobilization of Cd and Zn is best described as a concentration-dependent precipitation process governed by the coupled effects of dissolved metal activity, reduced sulfur availability, supersaturation dynamics, nucleation behavior, aggregation processes, and matrix demand. The results of this study indicate that the higher-concentration systems produced CPS-derived precipitates with lower acid-extractable fractions, whereas the lower-concentration systems required disproportionately higher CPS-to-metal ratios to exceed the apparent precipitation threshold and achieve comparable immobilization of Cd and Zn (see Fig. 3). Thus, the crystallization interpretation and framework provide a mechanistic basis for the experimentally identified $C_{CPS,Cri}$ and $C_{CPS,Opt}$ thresholds, while also emphasizing that practical CPS dosing should account for both thermodynamic saturation and kinetic limitations.

5. Implications for concentration-adjusted CPS remediation design

The results indicate that CPS dosing should be adjusted to not only dissolved Cd and Zn concentrations, but also site-specific geochemical demand. A uniform CPS dosage may generate different precipitation regimes across heterogeneous plumes because metal concentration, oxidant demand, pH buffering, sulfate abundance, and competing ions vary spatially. In high-concentration source zones, elevated metal activity can promote rapid supersaturation once sufficient reduced sulfur is available, favoring formation of lower-extractability sulfide-associated precipitates. In contrast, marginally contaminated plume zones may require proportionally higher CPS-to-metal ratios because part of the injected CPS is consumed by background reactions before effective $CdS_{(s)}$ and $ZnS_{(s)}$ precipitation is achieved. Therefore, field-scale CPS application should combine concentration mapping, pH-ORP and/or pH-Eh profiling, sulfate/sulfide monitoring, oxidant-demand assessment, and site-specific treatability testing to identify the threshold-to-optimal dosing window while avoiding unnecessary geochemical disturbance.

6. Conclusions

This study evaluated CPS remediation for Cd- and Zn-contaminated groundwater across distinct concentration ranges and developed a concentration-dependent dosing framework linking sulfide availability, metal supersaturation, metal precipitate formation, and post-remediation metal extractability. With respect to the stated objectives, the principal conclusions are as follows.

Remediation with CPS shifted acidic, oxidizing groundwater ($3.86 \leq pH \leq 4.51$, $105\ mV \leq Eh \leq 182\ mV$) toward more alkaline, reducing, and sulfide-favoring conditions ($7.35 \leq pH \leq 9.03$, $-141\ mV \leq Eh \leq -31.4\ mV$). However, Cd and Zn removal was not governed solely by pH or Eh changes. Substantial metal removal occurred only when CPS addition generated sufficient reduced sulfur activity to exceed the apparent metal-sulfide precipitation threshold, expressed conceptually as $\Omega_{MeS} = \{Me^{2+}\}\{S^{2-}\}/K_{sp,MeS} > 1$. Accordingly, the critical CPS concentration, $C_{CPS,Cri}$, was defined as the operational precipitation-onset

dosage at which the CPS-induced pH/Eh transition coincided with rapid Cd and Zn removal, whereas the optimal CPS concentration, $C_{CPS,Opt}$, represented the lowest dosage that achieved near-maximum removal without additional CPS input.

The required CPS dosage was concentration-dependent. Higher initial Cd and Zn concentrations required greater absolute CPS dosages because of higher metal mass loading and greater matrix demand. In contrast, groundwater with lower metals concentrations required disproportionately higher CPS-to-metal ratios because a portion of the injected CPS was consumed by oxidant demand, sulfur transformation reactions, pH buffering, and competing matrix reactions before effective $CdS_{(s)}$ and $ZnS_{(s)}$ precipitation was achieved. These results indicate that CPS dosage should be based on not only stoichiometric metal demand, but also the initial metals concentrations and site-specific geochemical demand.

Multi-technique solid-phase characterization confirmed that CPS remediation immobilized Cd and Zn primarily via sulfidation. The SEM-EDS and TEM-EDS results indicated spatial association of Cd, Zn, S, and Ca within precipitate-rich domains, while XRD identified crystalline $ZnS_{(s)}$, gypsum ($CaSO_4{\cdot}2\ H_2O$), and elemental sulfur (S^0). The results of the XPS further confirmed sulfide, elemental sulfur, and sulfate components, together with Cd- and Zn-bearing sulfide coordination environments. These results demonstrate that CPS remediation generated mixed sulfide-sulfate-sulfur precipitate assemblages, with metal sulfide formation serving as the dominant immobilization pathway.

The results of mass-balance, acid-extraction, and sequential-extraction showed that CPS-derived Cd and Zn precipitates were primarily retained as low-extractability solid phases under the tested conditions. Most immobilized Cd and Zn occurred in sulfide-associated and residual fractions, whereas exchangeable, carbonate-bound, and oxide-bound fractions were comparatively minor. The lower extractability observed at higher initial metal concentrations is consistent with supersaturation-enhanced precipitation, aggregation, and growth of sulfide-rich solids.

Overall, the proposed framework advances CPS remediation from empirical dosage selection toward a concentration-adjusted design strategy that links $C_{CPS,Cri}$, $C_{CPS,Opt}$, initial metal concentration, supersaturation behavior, and precipitate extractability. Therefore, field-scale application should consider not only stoichiometric sulfur demand, but also hydrogeochemical heterogeneity, matrix demand, and the long-term stability of CPS-derived precipitates under fluctuating pH and redox conditions.

CRediT authorship contribution statement

Won Seok Park: Supervision, Resources, Funding acquisition. **Jiwon Choi:** Writing – original draft, Investigation, Data curation. **Jin Chul Joo:** Writing – review & editing, Writing – original draft, Validation, Investigation, Data curation, Conceptualization. **Charles D. Shackelford:** Writing – review & editing, Validation, Supervision. **Kyoungphile Nam:** Writing – review & editing, Supervision, Project administration, Funding acquisition, Conceptualization. **Hyeon Woo Go:** Visualization, Investigation, Formal analysis, Data curation. **Dong Jun Kim:** Visualization, Investigation, Data curation.

Declaration of Competing Interest

The authors declare that they have no known competing financial interests or personal relationships that could have appeared to influence the work reported in this paper.

Acknowledgments

This research was supported by the Hanbat National University (HBNU) Financial Accounting Research Fund for 2025. The opinions expressed in this paper are solely those of the authors and are not necessarily consistent with the policies or opinions of the HBNU.

Appendix A. Supporting information

Supplementary data associated with this article can be found in the online version at doi:10.1016/j.jece.2026.124647.

Data availability

Data will be made available on request.

References

[1] G. Jiang, B. Peng, Y. Liang, L. Chai, Q. Wang, Q. Li, M. Hu, Recovery of valuable metals from zinc leaching residue by sulfate roasting and water leaching, Trans. Nonferrous Met. Soc. China 27 (5) (2017) 1180–1187, https://doi.org/10.1016/S1003-6326(17)60138-9.
[2] J. Briffa, E. Sinagra, R. Blundell, Heavy metal pollution in the environment and their toxicological effects on humans, Heliyon 6 (9) (2020) e04691, https://doi.org/10.1016/j.heliyon.2020.e04691.
[3] Y.M. Wang, T.C. Chen, K.J. Yeh, M.F. Shue, Stabilization of an elevated heavy metal contaminated site, J. Hazard. Mater. 88 (1) (2001) 63–74, https://doi.org/10.1016/S0304-3894(01)00289-8.
[4] S. Xue, W. Ke, J. Zeng, C.B. Tabelin, Y. Xie, L. Tang, C. Xiang, J. Jiang, Pollution prediction for heavy metals in soil-groundwater systems at smelting sites, Chem. Eng. J. 473 (2023) 145499, https://doi.org/10.1016/j.cej.2023.145499.
[5] A. Kubier, R.T. Wilkin, T. Pichler, Cadmium in soils and groundwater: A review, Appl. Geochem. 108 (2019) 104388, https://doi.org/10.1016/j.apgeochem.2019.104388.
[6] Q. Li, Y. Wang, Y. Li, L. Li, M. Tang, W. Hu, L. Chen, S. Ai, Speciation of heavy metals in soils and their immobilization at micro-scale interfaces: a review, Sci. Total. Environ. 825 (2022) 153862, https://doi.org/10.1016/j.scitotenv.2022.153862.
[7] P.B. Tchounwou, C.G. Yedjou, A.K. Patlolla, D.J. Sutton, Heavy metal toxicity and the environment, in: Molecular, Clinical and Environmental Toxicology, 101, Springer, *Basel*, 2012, pp. 133–164, https://doi.org/10.1007/978-3-7643-8340-4_6.
[8] USEPA (United States Environmental Protection Agency), Basics of Pump-and-Treat Ground-Water Remediation Technology, EPA/600/8-90/003, Office of Research and Development, U.S. Environment Protection Agency, Ada, Oklahoma 74820, 1990.
[9] M.A. Hashim, S. Mukhopadhyay, J.N. Sahu, B. Sengupta, Remediation technologies for heavy metal contaminated groundwater, J. Environ. Manag. 92 (10) (2011) 2355–2388, https://doi.org/10.1016/j.jenvman.2011.06.009.
[10] E. Zulu, S. Ramasamy, K.K. Sikhwivhilu, S. Syampungani, A comprehensive review of recent advances in membrane innovations for efficient heavy metal removal from mine effluents, Sci. Afr. 27 (2025) e02510, https://doi.org/10.1016/j.sciaf.2024.e02510.
[11] V.R. Vermeul, M.D. Williams, J.E. Szecsody, J.S. Fruchter, C.R. Cole, J. E. Amonette, Creation of a subsurface permeable reactive barrier using in situ redox manipulation, in: Handbook of Groundwater Remediation Using Permeable Reactive Barriers, Academic Press, 2003, pp. 163–192, https://doi.org/10.1016/B978-012513563-4/50010-4.
[12] T. Mpouras, N. Papassiopi, K. Lagkouvardos, C. Mystrioti, D. Dermatas, Evaluation of calcium polysulfide as a reducing agent for the restoration of a Cr(VI)-contaminated aquifer, Bull. Environ. Contam. Toxicol. 106 (3) (2021) 435–440, https://doi.org/10.1007/s00128-020-02890-1.
[13] A.E. Lewis, Review of metal sulphide precipitation, Hydrometallurgy 104 (2) (2010) 222–234, https://doi.org/10.1016/j.hydromet.2010.06.010.
[14] H. Estay, L. Barros, E. Troncoso, Metal sulfide precipitation: recent breakthroughs and future outlooks, Minerals 11 (12) (2021) 1385, https://doi.org/10.3390/min11121385.
[15] X. Zhang, L. Zeng, Y. Wang, J. Tian, J. Wang, W. Sun, H. Han, Y. Yang, Selective separation of metals from wastewater using sulfide precipitation: a critical review in agents, operational factors and particle aggregation, J. Environ. Manag. 344 (2023) 118462, https://doi.org/10.1016/j.jenvman.2023.118462.
[16] S. Cheng, X. Hong, H. Tang, Y. Chu, C. Huang, Preparation of calcium polysulfide to remediate groundwater contaminated by hexavalent chromium, Proc. AMMMS (2018) 518–524, https://doi.org/10.12783/dtcse/ammms2018/27335.
[17] S. Hu, D. Li, Y. Man, Y. Wen, C. Huang, Evaluation of remediation of Cr(VI)-contaminated soils by calcium polysulfide: Long-term stabilization and mechanism studies, Sci. Total. Environ. 790 (2021) 148140, https://doi.org/10.1016/j.scitotenv.2021.148140.
[18] S.M. Dahlawi, S. Siddiqui, Calcium polysulphide, its applications and emerging risk of environmental pollution—a review article, Environ. Sci. Pollut. Res. 24 (1) (2017) 92–102, https://doi.org/10.1007/s11356-016-7842-3.
[19] H.W. Go, J.C. Joo, K. Nam, H.S. Moon, S. Yoon, D.H. Lee, S.Y. Jang, Feasibility evaluation for remediation of groundwater contaminated with heavy metal using calcium polysulfide in homogeneous media, J. Soil. Groundw. Environ. 28 (1) (2023) 1–14, https://doi.org/10.7857/JSGE.2023.28.1.001.
[20] S. Yoon, S. Jeong, C. Moon, K. Nam, Removal of cadmium and zinc by calcium polysulfide in acidic groundwater: Injection ratio and precipitation mechanism,

Chemosphere 364 (2024) 143219, https://doi.org/10.1016/j.chemosphere.2024.143219.
[21] J. Choi, J.C. Joo, K. Nam, H.W. Go, W.S. Park, I. Lee, D.J. Kim, Optimal injection dosage determination of calcium polysulfide (CPS) for remediation of groundwater contaminated with complex heavy metals with various concentration ranges, J. Soil. Groundw. Environ. 29 (6) (2024) 49–59, https://doi.org/10.7857/JSGE.2024.29.6.049.
[22] J.C. Joo, H.W. Go, C.D. Shackelford, K. Nam, H.S. Moon, J. Choi, J. Kim, Remediating zinc-contaminated groundwater with calcium polysulfide using model porous media and simulated groundwater, J. Hazard. Mater. 491 (2025) 137840, https://doi.org/10.1016/j.jhazmat.2025.137840.
[23] J.C. Joo, H.W. Go, C.D. Shackelford, K. Nam, H.S. Moon, D.J. Kim, S.J. Kim, Laboratory evaluation of calcium polysulfide for immobilization of metals from contaminated groundwater under site-specific conditions, J. Environ. Chem. Eng. 13 (6) (2025) 120217, https://doi.org/10.1016/j.jece.2025.120217.
[24] A. Pohl, Removal of heavy metal ions from water and wastewaters by sulfur-containing precipitation agents, Water Air Soil. Pollut. 231 (10) (2020) 503, https://doi.org/10.1007/s11270-020-04863-w.
[25] M. Chrysochoou, D.R. Ferreira, C.P. Johnston, Calcium polysulfide treatment of Cr (VI)-contaminated soil, J. Hazard. Mater. 179 (1–3) (2010) 650–657, https://doi.org/10.1016/j.jhazmat.2010.03.052.
[26] USEPA (United States Environmental Protection Agency), Method 3051A: Microwave Assisted Acid Digestion of Sediments, Sludges, Soils, and Oils, Revision 1. Washington, DC, 2007.
[27] A. Tessier, P.G.C. Campbell, M. Bisson, Sequential extraction procedure for the speciation of particulate trace metals, Anal. Chem. 51 (7) (1979) 844–851, https://doi.org/10.1021/ac50043a017.
[28] C. Tu, F. Guan, Y. Sun, P. Guo, Y. Liu, L. Li, K.G. Scheckel, Y. Luo, Stabilizing effects on a cadmium polluted coastal wetland soil using calcium polysulphide, Geoderma 332 (2018) 190–197, https://doi.org/10.1016/j.geoderma.2018.07.013.